JOURNAL OF PROPULSION AND POWER
Vol. 17, No. 6, November–December 2001

Quasi-One-Dimensional High-Speed Engine Model with Finite-Rate Chemistry

Timothy F. O'Brien,* Ryan P. Starkey,† and Mark J. Lewis‡
University of Maryland, College Park, Maryland 20742

The quasi-one-dimensional equations of fluid motion are coupled with the equations for finite-rate chemistry to model high-speed engine flowfields. The model was developed for rapid vehicle design and optimization, where a wide range of engine inlet conditions may be encountered. Incorporating the timescales of fuel mixing and ignition are crucial for accurate prediction of combustor performance, especially for nonhydrogen fuels and off-design conditions (where equilibrium assumptions are invalid). The effects of area change, friction, mass injection, fuel mixing, and heat transfer to the combustor walls are included. The resulting model is compared to experimental results for hydrogen-fueled scramjet engines to demonstrate the ability to predict wall pressure profiles and fuel ignition point. Application to a rocket-based combined-cycle engine and a hydrocarbon scramjet missile engine are discussed. The model presented predicts peak pressure and fuel ignition accurately, as well as flowfield pressures in regions where boundary-layer separation is not present.

Nomenclature

A	=	cross-sectional area of engine, m^2
$a-d$, f	=	curvefit constants
a_{1i-5i}	=	curvefit constants
C_f	=	friction coefficient
C_H	=	Stanton number
c_p	=	specific heat at constant pressure, J/(kg-K)
D	=	drag, N
$\mathcal{D}$	=	hydraulic diameter, m
f_{st}	=	stoichiometric fuel/air ratio
g	=	gravitational acceleration, m/s^2
h	=	enthalpy per unit mass, J/kg
I_{sp}	=	specific impulse, s
L	=	length, m
M	=	Mach number
$\underline{MW}$	=	molecular weight, kg/kmol
$\overline{MW}$	=	mixture molecular weight, kg/kmol
$\dot{m}$	=	mass flow rate, kg/s
P_w	=	wetted perimeter, m
Pr	=	Prandtl number
p	=	pressure, N/m^2
$\dot{Q}$	=	heat-transfer rate, J/s
R_u	=	universal gas constant, J/(kmol-K)
T	=	temperature, K; thrust, N
U	=	velocity, m/s
V	=	volume, m^3
X	=	mole fraction
x	=	axial coordinate, m
$\bar{x}$	=	nondimensional axial coordinate
Y	=	mass fraction
γ	=	ratio of specific heats
Δx	=	control volume increment of x
ε	=	ratio of gas injection velocity to freestream velocity
η	=	efficiency
ρ	=	density, kg/m^3
ϕ	=	equivalence ratio
$\dot{\omega}$	=	molar production rate, kmol/(s-m^3)

Subscripts

added	=	species added for mass/fuel injection
aw	=	adiabatic wall
comb	=	combustor
e	=	end
eff	=	effective
f	=	total fuel available
i	=	ith species
inj	=	injection
mix	=	mixing
o	=	total or stagnation conditions
r	=	available for reaction
s	=	start
st	=	stoichiometric conditions
w	=	wall
x, Δx	=	control volume descriptors
∞	=	freestream conditions

Superscripts

$''$	=	per unit area
$'''$	=	per unit volume
$*$	=	evaluated at the reference temperature

Introduction

THE prediction of high-speed vehicle performance depends on the accurate modeling of both the aerodynamics of the airframe and the flow conditions within the combustor. If optimization of the vehicle for range, payload, etc. is desired, then a rapid means of predicting the vehicle flowfield will make optimization a less computationally expensive endeavor. Further, if trajectory calculations are needed, a rapid means of predicting the vehicle performance allows for a quicker analysis.

A quasi-one-dimensional combustor flowfield model that includes finite-rate chemistry is presented in this paper. The inclusion of chemical kinetics allows for a prediction of fuel ignition, a finite-rate process that inherently cannot be predicted using equilibrium methods. The inclusion of chemistry also allows for off-design calculations to determine necessary conditions for the fuel to burn and under what conditions will cause the combustor to choke. These prediction capabilities are crucial in flowfield regimes where the limits of the scramjet concept are encountered (i.e., hydrocarbon missile scramjets, ram/scram transition, etc.).

Received 14 October 2000; revision received 24 January 2001; accepted for publication 12 February 2001.

*Graduate Research Assistant, Department of Aerospace Engineering; genghis@eng.umd.edu. Student Member AIAA.

†Faculty Research Assistant, Department of Aerospace Engineering; rstarkey@eng.umd.edu. Member AIAA.

‡Professor, Department of Aerospace Engineering; lewis@eng.umd.edu. Associate Fellow AIAA.

A series of ordinary differential equations that model the governing equations of motion will be presented. Along with a user-specified cross-sectional area profile, mass and reaction mixing profile, viscous model, and a reaction mechanism, the ordinary differential equations are integrated to solve for the combustor flowfield. Two example hydrogen-fueled scramjet experiments are compared to the model to demonstrate the ignition point and pressure profile prediction capabilities. Also presented are two applications of the combustor model: a hydrogen-fueled rocket-based combined-cycle engine and a hydrocarbon-fueled scramjet missile engine. These applications represent two engine profiles where prediction of fuel ignition point is crucial in calculating the thrust generated by the combustor and equilibrium assumptions are inadequate.

Governing Equations for the Model

The governing equations for the engine model are based on the following assumptions: 1) quasi-one-dimensional flow, where all variables (including area) are functions in the x direction only, 2) steady-state flow, and 3) the flow behaves as a perfect gas.

Continuity

The quasi-one-dimensional, steady continuity equation can be stated as

$$\dot{m} = \rho U A \tag{1}$$

The continuity equation (1) can be expressed in differential form[1] as

$$\frac{1}{\dot{m}}\frac{\mathrm{d}\dot{m}}{\mathrm{d}x} = \frac{1}{\rho}\frac{\mathrm{d}\rho}{\mathrm{d}x} + \frac{1}{U}\frac{\mathrm{d}U}{\mathrm{d}x} + \frac{1}{A}\frac{\mathrm{d}A}{\mathrm{d}x} \tag{2}$$

The differential continuity equation (2) allows for variation in cross-sectional area ($\mathrm{d}A/\mathrm{d}x$) of the combustor (geometry effects) and mass injection ($\mathrm{d}\dot{m}/\mathrm{d}x$) of fuel, pilot, or other bleeds. Both $\mathrm{d}A/\mathrm{d}x$ and $\mathrm{d}\dot{m}/\mathrm{d}x$ are prescribed by the user.

When mass is added to the system, it is assumed that the mass is instantaneously mixed with the engine flowfield. However, it will take a finite amount of time for the mass added to the system to completely affect the freestream in a quasi-one-dimensional sense. To model this effect, any mass that is injected from a discrete location is assumed to follow a user-prescribed mass mixing profile (or injector arrangement). Mass injected from an injection port is added to the flowfield incrementally in the x direction by the mass-addition term $\mathrm{d}\dot{m}/\mathrm{d}x$. In this manner, mass is added to the flow as it travels through the engine until the full amount of mass injected is present. This mass-addition term should not be confused with fuel mixing. Although mass and fuel mixing can be treated as the same mechanism, they are not inherently the same. The mass-addition term is solely used to add more mass to the engine flowfield. Fuel mixing (to be discussed in more detail in the following sections) is prescribed to make the injected fuel available for reaction (i.e., enough mixing has occurred between the air and fuel such that combustion can take place).

Momentum

The quasi-one-dimensional momentum equation in differential form[1] can be expressed as

$$\frac{1}{p}\frac{\mathrm{d}p}{\mathrm{d}x} + \frac{\gamma M^2}{2U^2}\frac{\mathrm{d}U^2}{\mathrm{d}x} + \frac{2\gamma M^2 C_f}{\mathcal{D}} + \frac{\gamma M^2(1-\varepsilon)}{\dot{m}}\frac{\mathrm{d}\dot{m}}{\mathrm{d}x} = 0 \tag{3}$$

where ε is the ratio of the velocity of gas injection in the x direction over the velocity of the flowfield

$$\varepsilon \equiv U_i/U_\infty \tag{4}$$

Equation (4) accounts for angled fuel injection ($\varepsilon = 0$ for normal fuel injection). The momentum equation [Eq. (3)] accounts for viscosity in the flow as a momentum deficit. The friction coefficient is prescribed by the user and can be found from experimental results or by some analytical or empirical method. The friction coefficient used in the examples and application problems to follow is calculated using Eckert's reference-temperature method[2] assuming fully turbulent flow.[3] The viscosity is evaluated at the reference temperature by using Sutherland's Law.[3] The hydraulic diameter of a rectangular engine cross section can be found from

$$\mathcal{D} \equiv 4A/P_w \tag{5}$$

Equation of State

Assuming a perfect gas, the equation of state can be expressed as

$$p = \rho R_u T/\overline{MW} \tag{6}$$

Expressing the equation of state in differential form[4] yields

$$\frac{1}{p}\frac{\mathrm{d}p}{\mathrm{d}x} = \frac{1}{\rho}\frac{\mathrm{d}\rho}{\mathrm{d}x} + \frac{1}{T}\frac{\mathrm{d}T}{\mathrm{d}x} - \frac{1}{\overline{MW}}\frac{\mathrm{d}\overline{MW}}{\mathrm{d}x} \tag{7}$$

The preceding form for the equation of state allows the inclusion of the chemical changes caused by mass injection and combustion.

Mixture Molecular Weight

The mixture molecular weight can be expressed in terms of the mass fraction as

$$\overline{MW} = 1 \Big/ \sum_i \frac{Y_i}{MW_i} \tag{8}$$

The differential form of the mixture molecular weight has the form[4]

$$\frac{\mathrm{d}\overline{MW}}{\mathrm{d}x} = -\overline{MW}^2\left(\sum_i \frac{1}{MW_i}\frac{\mathrm{d}Y_i}{\mathrm{d}x}\right) \tag{9}$$

Species Conservation

The derivation of the species conservation equation is based on derivations given by Turns.[4] The finite control volume for the quasi-one-dimensional, steady case is shown in Fig. 1. Conservation of species i in Fig. 1 is found to be

$$[\dot{m}_i'' A]_{x+\Delta x} - [\dot{m}_i'' A]_x = \dot{m}_i''' V + \dot{m}_{i,\text{added}} \tag{10}$$

The left-hand side of Eq. (10) is the net mass flow of species i leaving the control volume. The first term on the right-hand side of Eq. (10) is a source or sink term caused by chemical reaction within the control volume. The second term on the right-hand side is a source term that models mass/fuel injection.

Neglecting molecular diffusion in the flow direction, Eq. (10) can be expressed as

$$[Y_i \dot{m}'' A]_{x+\Delta x} - [Y_i \dot{m}'' A]_x = \dot{m}_i''' A \Delta x + \dot{m}_{i,\text{added}} \tag{11}$$

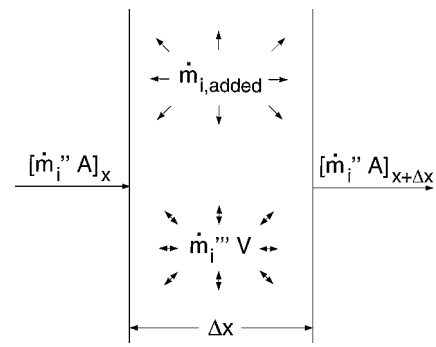

Fig. 1 Quasi-one-dimensional control volume for species conservation derivation.

where the volume of the quasi-one-dimensional control volume is $A\Delta x$. As Δx becomes infinitesimally small, Eq. (11) can be expressed in differential form as

$$\frac{1}{A}\frac{\mathrm{d}[Y_i \dot{m}'' A]}{\mathrm{d}x} = \dot{m}_i''' + \frac{1}{A}\frac{\mathrm{d}\dot{m}_{i,\text{added}}}{\mathrm{d}x} \tag{12}$$

The source term $\dot{m}_i'''$ can be expressed as

$$\dot{m}_i''' = \dot{\omega}_i M W_i \tag{13}$$

Separating the mass fraction from the differential in Eq. (12) and substituting Eq. (13) yields the differential species conservation equation

$$\frac{\mathrm{d}Y_i}{\mathrm{d}x} = \frac{\dot{\omega}_{i,\text{mix}} M W_i}{\rho U} + \frac{1}{\dot{m}}\frac{\mathrm{d}\dot{m}_{i,\text{added}}}{\mathrm{d}x} - \frac{Y_i}{\dot{m}}\frac{\mathrm{d}\dot{m}}{\mathrm{d}x} \tag{14}$$

Equation (14) states that the change in mass fraction of species i is a function of the rate of production/destruction of species i, the amount of species i added, and the total amount of mass added.

The subscript $()_{\text{mix}}$ has been added to the production rate in Eq. (14) to denote fuel mixing. In addition to the prescribed mass-addition profile $\mathrm{d}\dot{m}/\mathrm{d}x$, a fuel-mixing profile may be prescribed to model when the fuel that has been injected is available for reaction. This mixing profile can take the form of a mixing efficiency (where a certain percentage of fuel injected is never available for reaction) and/or a mixing length (where after the fuel has been added to the flow in a mass sense, a finite amount of mixing time is necessary before reaction can begin to occur).

An example injection scheme is shown in Fig. 2. Fuel injection is assumed to occur over a length L_{inj} from $x_{\text{inj},s}$ to $x_{\text{inj},e}$ to model staggered fuel injection ports and finite mass mixing time. A prescribed mixing length L_{mix} is given to tell the flowfield how long the fuel must remain in the combustor before reaction can begin. Until the fuel reaches the point $x_{\text{inj},s} + L_{\text{mix}}$, only mixing is assumed to occur, and the fuel production rate $\dot{\omega}_i$ is set to zero. When the mixing length has been reached, reaction can begin and continue until either the end of the combustor or equilibrium has been reached. When reaction begins, a mixing efficiency η_{mix} may be prescribed so that at any point a certain percentage of the initial fuel injected is not available for reaction. The mixing efficiency is prescribed to model unmixed fuel in the combustor but can also represent inefficiencies and losses as a result of fuel injection.

Energy

The derivation of the energy equation is partially based on the formulation presented by Turns.[4] The finite control volume for the

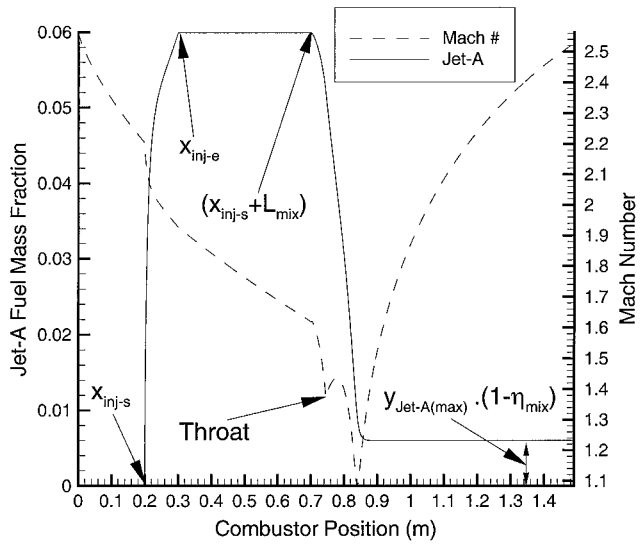

Fig. 2 Fuel mass fractions for sample injection and mixing profiles in a Jet-A scramjet engine for missile application.

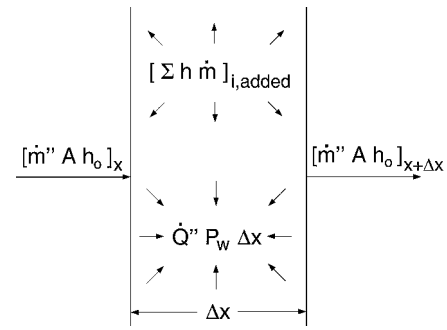

Fig. 3 Quasi-one-dimensional control volume for energy derivation.

quasi-one-dimensional, steady energy equation derivation is shown in Fig. 3. Neglecting axial heat conduction, axial species diffusion, radiation, and work done on the control volume, conservation of energy in Fig. 3 yields the following equation:

$$[\dot{m}'' A h_o]_{x+\Delta x} - [\dot{m}'' A h_o]_x = \left[\sum_i h_i \dot{m}_i\right]_{\text{added}} - \dot{Q}'' P_w \Delta_x \tag{15}$$

$$h_o \equiv h + U^2/2 \tag{16}$$

The left-hand side of Eq. (15) is the net amount of energy flow leaving the control volume. The first term on the right-hand side of Eq. (15) is a source term for enthalpy addition caused by fuel injection and assumes thermal equilibrium between the fuel and the flowfield. The second term on the right-hand side of Eq. (15) is a sink term for heat transferred to the engine wall. As Δx becomes infinitesimally small, the energy equation becomes

$$\frac{\mathrm{d}[\dot{m}'' A h_o]}{\mathrm{d}x} = \frac{\mathrm{d}\left[\sum_i h_i \dot{m}_i\right]_{\text{added}}}{\mathrm{d}x} - \dot{Q}'' P_w \tag{17}$$

Using the chain rule, Eq. (17) is rewritten as

$$\frac{\mathrm{d}h}{\mathrm{d}x} = \frac{1}{\dot{m}}\frac{\mathrm{d}\left[\sum_i h_i \dot{m}_i\right]_{\text{added}}}{\mathrm{d}x} - \frac{\dot{Q}'' P_w}{\dot{m}'' A} - \frac{h_o}{\dot{m}}\frac{\mathrm{d}\dot{m}}{\mathrm{d}x} - U\frac{\mathrm{d}U}{\mathrm{d}x} \tag{18}$$

The enthalpy of the flowfield can be written in terms of the enthalpy of each species

$$h = \sum_i c_{p_i} T Y_i \tag{19}$$

where the flowfield is assumed to be thermally perfect so that enthalpy is not a function of flowfield pressure. The derivative of enthalpy as a function of axial distance can then be found from Eq. (19):

$$\frac{\mathrm{d}h}{\mathrm{d}x} = \sum_i \left[h_i \frac{\mathrm{d}Y_i}{\mathrm{d}x} + T Y_i \frac{\mathrm{d}c_{p_i}}{\mathrm{d}x}\right] + c_p \frac{\mathrm{d}T}{\mathrm{d}x} \tag{20}$$

The specific heat of species i can be represented by a curvefit with respect to temperature in the following form

$$c_{p_i} = (R_u/MW_i)\left(a_{1i} + a_{2i}T + a_{3i}T^2 + a_{4i}T^3 + a_{5i}T^4\right) \tag{21}$$

Equation (21) is in the form used by CHEMKIN II.[5] Assuming the constants $a_{1i} - a_{5i}$ are weak functions of temperature, the derivative of c_{p_i} with respect to axial distance yields an equation in terms of temperature derivative

$$\frac{\mathrm{d}c_{p_i}}{\mathrm{d}x} = \tilde{c}_{p_i}\frac{\mathrm{d}T}{\mathrm{d}x} \tag{22}$$

where

$$\tilde{c}_{p_i} \equiv (R_u/MW_i)\left(a_{2i} + 2a_{3i}T + 3a_{4i}T^2 + 4a_{5i}T^3\right) \tag{23}$$

Substituting Eq. (22) into Eq. (20) yields the final form of the derivative of enthalpy:

$$\frac{\mathrm{d}h}{\mathrm{d}x} = \tilde{c}_p \frac{\mathrm{d}T}{\mathrm{d}x} + \sum_i h_i \frac{\mathrm{d}Y_i}{\mathrm{d}x} \tag{24}$$

$$\tilde{c}_p \equiv c_p + \sum_i T\tilde{c}_{p_i} Y_i \tag{25}$$

In a similar manner, the derivative of enthalpy of species i can be written as

$$\frac{\mathrm{d}h_i}{\mathrm{d}x} = \left(c_{p_i} + \tilde{c}_{p_i} T\right)\frac{\mathrm{d}T}{\mathrm{d}x} \tag{26}$$

The heat-transfer term [second term on the right-hand side of Eq. (18)] is calculated from the definition of the Stanton number

$$C_H \equiv \dot{Q}''/\rho U(h_{\mathrm{aw}} - h_w) \tag{27}$$

The Stanton number can be related to the friction coefficient by Reynolds analogy

$$C_H = C_f/2Pr^{\frac{2}{3}} \tag{28}$$

where Pr is the Prandtl number (assumed in the given examples to be a constant value of 0.71). Substituting Eq. (28) into Eq. (27), the second term in Eq. (18) can be written as

$$\frac{\dot{Q}'' P_w}{\dot{m}'' A} = \frac{2C_f c_p(T_{\mathrm{aw}} - T_w)}{Pr^{\frac{2}{3}}\mathcal{D}A} \tag{29}$$

It is assumed that the wall enthalpies can be written as a function of wall and adiabatic wall temperatures and freestream specific heat at constant pressure, where adiabatic wall temperature can be calculated from[6]

$$T_{\mathrm{aw}} = T\left[1 + (Pr^*)^{\frac{1}{3}}[(\gamma - 1)/2]M^2\right] \tag{30}$$

where Pr^* is the Prandtl number evaluated at the reference temperature. For the current study the reference Prandtl number is also assumed to have a value of 0.71. Finally, substituting Eqs. (24), (26), and (29) into Eq. (18) yields the quasi-one-dimensional, steady, differential energy equation

$$\frac{\mathrm{d}T}{\mathrm{d}x} = \frac{1}{\hat{c}_p}\left[-\sum_i h_i \frac{\mathrm{d}Y_i}{\mathrm{d}x} + \frac{1}{\dot{m}} \sum_i \left(h_i \frac{\mathrm{d}\dot{m}_i}{\mathrm{d}x} \right)_{\mathrm{added}} - \frac{2C_f c_p(T_{\mathrm{aw}} - T_w)}{Pr^{\frac{2}{3}}\mathcal{D}A} - \frac{h_o}{\dot{m}}\frac{\mathrm{d}\dot{m}}{\mathrm{d}x} - U\frac{\mathrm{d}U}{\mathrm{d}x} \right] \tag{31}$$

$$\hat{c}_p \equiv \tilde{c}_p - \frac{1}{\dot{m}}\left\{ \sum_i \left[\dot{m}_i\left(c_{p_i} + \tilde{c}_{p_i} T\right)\right]_{\mathrm{added}} \right\} \tag{32}$$

Solution Methodology

Equations (2), (3), (7), (9), (14), and (31) constitute a stiff set of ordinary differential equations (ODE) from the chemical production terms from combustion. Solution of these equations requires a stiff ODE solver that can account for differing timescales. The VODPK[7] code, developed by Lawrence Livermore National Lab, was used to accomplish this task. VODPK uses a backward-differentiation formula to integrate the set of stiff ODEs. Values for the individual chemical species molecular weight, specific heat, heat of formation, and reaction rates are obtained from CHEMKIN-II[5] for a user-supplied reaction mechanism.

For this study two types of fuel are investigated: hydrogen and Jet-A. The hydrogen/air mechanism used was proposed by Jachimowski.[8] Jachimowski's mechanism contains 14 species, 33 reactions, includes nitrogen chemistry, and was specifically developed for application to high-speed combustion modeling. The Jet-A reaction mechanism used in this study is a subset of the full reaction mechanism from Kundu et al.[9] The reaction mechanism consists of 17 species and 14 reactions and was chosen because it has been validated by Chang[10] and Lewis and Chang.[11] The ambient air composition is assumed to be 78% nitrogen, 21% oxygen, and 1% argon by volume.

Solving Eqs. (2), (3), (7), and (31) for the derivative in velocity yields

$$\frac{\mathrm{d}U}{\mathrm{d}x} = \frac{1}{\alpha}\left\{ -\frac{1}{A}\frac{\mathrm{d}A}{\mathrm{d}x} + \frac{1 + \gamma M^2(1 - \varepsilon) - (h_o/\hat{h})}{\dot{m}}\frac{\mathrm{d}\dot{m}}{\mathrm{d}x} + \frac{1}{\hat{h}}\left[-\sum_i h_i \frac{\mathrm{d}Y_i}{\mathrm{d}x} + \frac{1}{\dot{m}}\sum_i \left(h_i \frac{\mathrm{d}\dot{m}_i}{\mathrm{d}x} \right)_{\mathrm{added}} \right] - \frac{1}{MW}\frac{\mathrm{d}MW}{\mathrm{d}x} + \left[\gamma M^2 - \frac{c_p(T_{\mathrm{aw}} - T_w)}{\hat{h}Pr^{\frac{2}{3}}A} \right]\frac{2C_f}{\mathcal{D}} \right\} \tag{33}$$

$$\alpha \equiv (1/U)(1 - \gamma M^2 + U^2/\hat{h}) \tag{34}$$

$$\hat{h} \equiv \hat{c}_p T \tag{35}$$

Each term in Eq. (33) can be calculated or is a prescribed quantity. The first term in Eq. (33) is the cross-sectional area profile $\mathrm{d}A/\mathrm{d}x$, which is assumed to be prescribed by the user. The second term is the mass flow addition term $\mathrm{d}\dot{m}/\mathrm{d}x$ and represents the mass mixing profile prescribed by the user. The quantity $\hat{h}$ can be calculated using CHEMKIN-II. Solution of the change in mixture molecular weight $\mathrm{d}\overline{MW}/\mathrm{d}x$ is found by first solving the species conservation equation [Eq. (14)]. Given the mixing profile and chemical information from CHEMKIN-II, Eq. (14) is a known quantity, which can then be substituted into Eq. (9) to solve for the change in mixture molecular weight. The friction terms involving the friction coefficient are all known quantities or can be calculated using CHEMKIN-II. The remaining terms in Eq. (33) are known quantities, quantities that have already been calculated, or quantities that can be calculated using CHEMKIN-II. Thus, the velocity derivative derived in Eq. (33) is a known quantity at a particular x location.

With knowledge of the velocity derivative, the density derivative may be found from the continuity equation [Eq. (2)]. The pressure derivative can be calculated from the momentum equation (3). The temperature derivative is then found from the equation of state [Eq. (7)]. The derivatives of all of the variables are then integrated using VODPK to find the flow solution.

Grid resolution is dependent on solution convergence using VODPK. Once a grid density is selected that allows for solution convergence in the ignition region, the overall flowfield is insensitive to further changes in grid density. The full engine flowfield can be calculated on the order of 1–2 s using a DEC-ALPHA computer. Thus, this method allows for rapid design of full vehicle concepts that include a detailed engine flowfield.

Example: Hydrogen-Fueled Scramjets

The combustor model just presented is now compared to a pair of experimental investigations into hydrogen-fueled scramjet engines. The first experiment is an axisymmetric, wall-injection scramjet investigated by Billig and Grenleski,[12] as shown in Fig. 4. The combustor consists of a constant-area circular cylinder (0.0038 m^2) that is 0.28 m long followed by a conical expansion section that is 0.61 m long, resulting in an area ratio of 2. Eight fuel injectors of diameter 2.64 mm each are evenly distributed along the circumference at the $x = 0$ location.

Reported incoming conditions into the combustor[12] are total temperature of 2180 K, total pressure of 3.13 $\mathrm{MN/m}^2$, Mach number

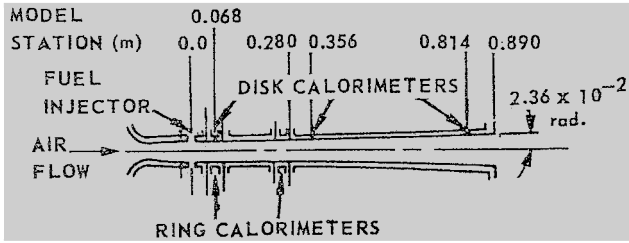

Fig. 4 Billig's experimental combustor configuration (from Ref. 12).

of 3.2, fuel temperature of 705 K, and an equivalence ratio of 0.5. Unfortunately, the chemical composition of the incoming air was not specifically given in Ref. 12; hence, the static properties entering the combustor can take on a wide range of values.[13,14] Reported experimental uncertainties for incoming pressure ranged from 52,000 to 55,000 N/m^2; incoming temperature from 820 to 940 K; and wall temperature from 450 to 550 K. The incoming air composition is assumed to be 78% N_2, 21% O_2, and 1% Ar by volume as already discussed. In this study the assumed incoming properties into the engine are $U = 1849$ m/s; $p = 52,000$ N/m^2; $T = 872$ K; $T_w = 500$ K; $\gamma = 1.346$; and $M = 3.19$. The assumed properties were selected to fall within the range of typical operating values reported in Ref. 12 and to closely match the reported incoming mass flow rate (an overprediction of approximately 6%). From the selected values the resulting error in total temperature is an overprediction of 10%, and the resulting error in total pressure is an underprediction of 14%. Considering the wide range of values reported in the literature, these errors are deemed acceptable for the current study.

The mixing model used for perpendicular injection of hydrogen is a curvefit of data originally reported by Rogers[15] and tabulated by Henry and Anderson[16]

$$\dot{m}_r = \dot{m}_f \frac{a\bar{x}^b \exp(c\bar{x})}{d\bar{x} + f} \tag{36}$$

$$\bar{x} \equiv \frac{x}{L_{\text{inj}}} \tag{37}$$

where L_{inj} is the length between $x_{\text{inj},s}$ and $x_{\text{inj},e}$, and the curvefit constants have the values $a = 1.1703$, $b = 0.62925$, $c = 0.42632$, $d = 1.4615$, and $f = 0.32655$. Taking the derivative of Eq. (36) yields

$$\frac{\mathrm{d}\dot{m}}{\mathrm{d}x} = \frac{\dot{m}_r}{L_{\text{inj}}}\left[\frac{cd\bar{x}^2 + (bd + cf - d)\bar{x} + bf}{\bar{x}(d\bar{x} + f)}\right] \tag{38}$$

where it is assumed for both scramjet test cases that the injection length is the same as the reaction mixing length.

Based on the preceding assumptions, the solution for the combustor flowfield is compared to the experimental results in Fig. 5. Good agreement is seen on the expansion region of the combustor, with an average error of under 15% compared to the experimental data. The maximum in pressure is predicted at the $x = 0.33$ m location (5 cm past the beginning of the expansion region). This location compares favorably with the experimental results for peak pressure location. Compared to an equilibrium solution, where the maximum in pressure would be just prior to the expansion region, the finite-rate solution allows for accurate prediction of fuel ignition while maintaining the peak pressure prediction found using equilibrium assumptions[12] (10% error compared to experimental results).

Prior to the ignition point, the combustor model fails to predict the pressure along the wall of the combustor. It is believed that boundary-layer burning might have occurred in this experiment,[14] which would increase the local pressure near the wall and act as a heat addition term. This effect, as well as any boundary-layer separation caused by injection, is not considered in the current combustor model. As a way to increase the heat addition, the injection length L_{inj} was assumed to be 2 cm in an attempt to model the preceding effects. A mixing efficiency of 96% was assumed for the preceding

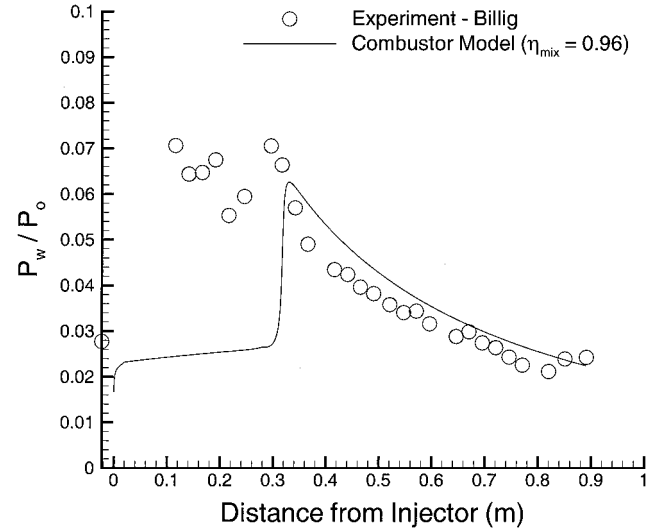

Fig. 5 Comparison of nondimensional wall pressure between experimental results from Ref. 12 and current combustor model.

calculations to yield a combustion efficiency of 94% (the same as reported in Ref. 12). Varying the mixing efficiency by ±4% resulted in a change in the peak pressure of ±3% and a change in pressure along the thrusting surface of ±2%.

The second experiment compared to the combustor model is that of the strut-based hydrogen-fueled scramjet tested by Anderson and Gooderum,[17] shown in Fig. 6. The apparatus consists of a strut injector, which injects hydrogen normal to the flowfield. The strut is located in a constant-area rectangular duct of height 3.81 cm and width 17 cm. The injectors are located 24 cm from the expansion section of the combustor, which has a length of 47.9 cm and an exit height of 7.62 cm. Ignoring the effects of the strut on the flowfield, the incoming flowfield has the following properties: $U = 1774.5$ m/s; $p = 75,777$ N/m^2; $p_o = 2.01$ MN/m^2; $T = 1031$ K; $M = 2.7$; $\gamma = 1.3$; an assumed $T_w = 500$ K; $L_{\text{inj}} = 0.6$ m; $\eta_{\text{mix}} = 95\%$; $f_{\text{st}} = 0.0349$; $\phi = 0.619$; and 22.3% O_2; 46.5% N_2; and 31.2% H_2O by volume. Reported experimental uncertainties are incoming Mach number of ±0.05, ±5% variation in local concentration of burner fuel and a local stagnation temperature variation of ±75 K.

The results from the combustor model are compared to the experimental results of Ref. 17 in Fig. 7. Good agreement is again seen on the expansion portion of the combustor wall with errors under 13%. Compared to the equilibrium solution reported by Anderson (see Fig. 7), a higher peak pressure is predicted, which comes closer to predicting the peak pressure measured in the experiment (error of approximately 7.5%). Prior to fuel ignition, the combustor model does not accurately predict wall pressures. The pressure data points in this region were influenced by boundary-layer separation from shock impingement from the strut and the influence of fuel injection and burning. These effects are not modeled in the quasi-one-dimensional combustor model. Heat transfer to the duct was calculated to be 0.587 MJ/s compared to the experimental result of 0.718 MJ/s, resulting in an 18% error. These results are in good agreement, considering that the combustor model did not include the length of duct prior to the strut injector, as well as the additional heat transfer from the shock wave/boundary-layer interaction.

The mixing efficiency for this case was selected to be 95%. Based on the variation of local burner fuel concentration just discussed, a mixing efficiency of 95% was deemed as an optimistic assumption of fuel mixing efficiency. If the mixing efficiency is raised above this amount, the flow was found to thermally choke. For a mixing efficiency of 90%, the peak pressure was reduced by 10%, and the pressure along the thrusting surface was reduced by approximately 3%.

Even with the vast limitations of quasi-one-dimensional flow, the current model does an excellent job of rapidly predicting the pressure profile on the expansion surface (vital for thrust prediction). It

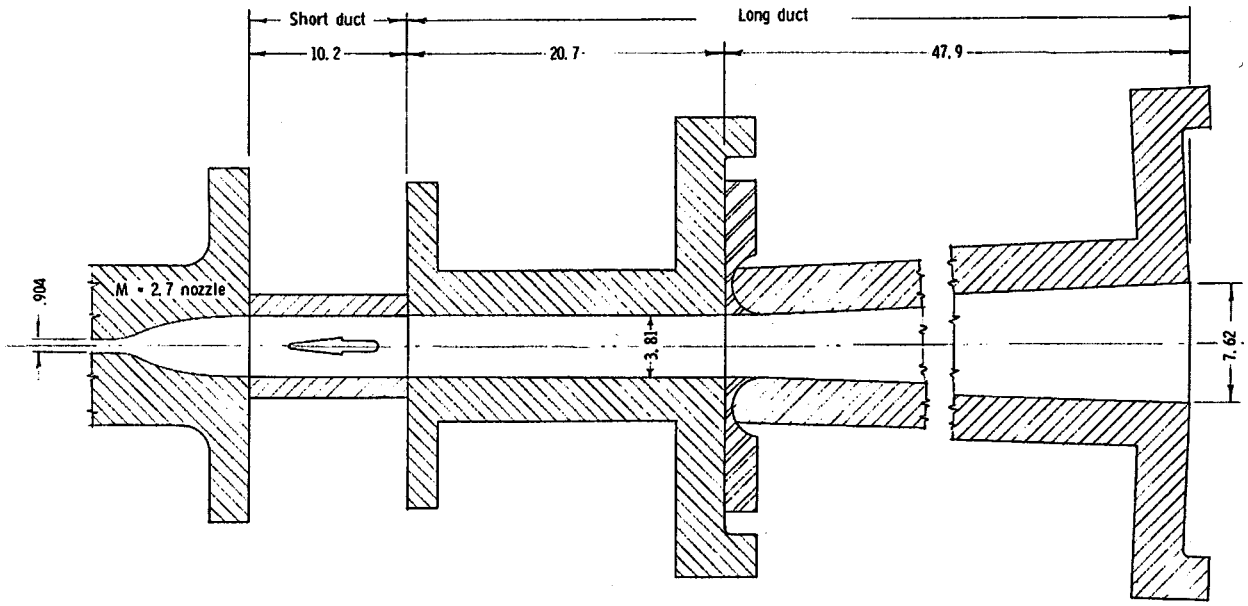

Fig. 6 Anderson and Gooderum's experimental combustor configuration (from Ref. 17).

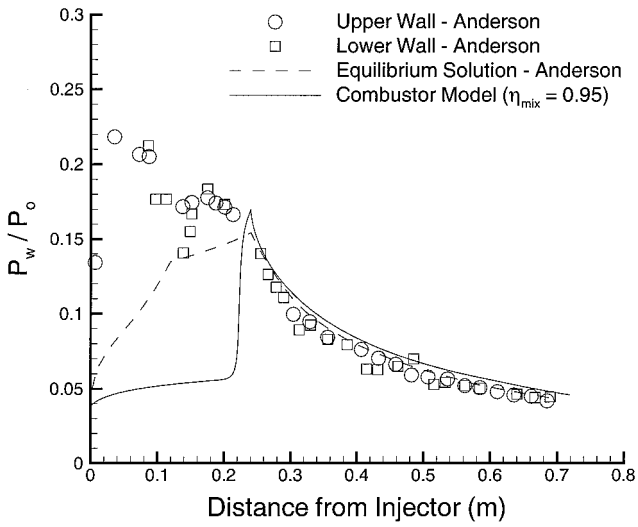

Fig. 7 Comparison of nondimensional wall pressure between experimental results from Ref. 17 and current combustor model.

also predicts fuel ignition location, even without the additional heat term caused by boundary-layer burning. Peak pressures calculated also compare quite well with experiment and earlier equilibrium solutions.

Application: Rocket-Based Combined-Cycle Engine

An application of the engine model is the scramjet mode of a rocket-based combined-cycle engine, shown in detail in Fig. 8. This engine model is loosely based on published descriptions of the Strutjet engine currently being tested by Aerojet.[18] The side view shows the complete propulsion system, which begins with a series of wedge compression ramps. The flow is turned back to parallel by the front of the engine cowl, with the cowl shock cancelling at the top of the combustor entrance. Two-dimensional flow is assumed as the flow passes into the strut injectors compression region (shown in the top view). The strut injectors compression region flow properties are calculated using oblique shock theory and Prandtl–Meyer flow assuming totally inviscid flow.[19] The area- averaged results from the compression region are then placed into the one-dimensional combustor model just presented to calculate the combustor flowfield. The chemical composition entering the combustor is assumed to be the chemical composition of air discussed in the Solution Methodology section. Gaseous hydrogen is injected normally at the end of the expansion portion of the strut (see Fig. 8). The fuel is assumed to be fully mixed by the end of the constant-area region between each set of struts and follows the same mixing profile as discussed in the preceding section. Following the constant-area region, a short but finite expansion is assumed to model the expansion caused by the base of the struts. Base pressure on the strut is assumed to be an average of the pressure before and after the expansion. Following the struts, the flow experiences a constant angle expansion for thrusting purposes followed by an internal and external nozzle. The nozzle portion of the propulsion system is calculated using the two-dimensional method of characteristics.[20]

Assuming freestream Mach number of 12 at an altitude of 36 km, the area-averaged incoming properties into the combustor are $p = 0.3$ atm, $T = 980$ K, $M = 5.73$, $\gamma = 1.34$, $\dot{m} = 722$ kg/s, $\phi = 1$, $\eta_{\text{mix}} = 95\%$ (assumed), $T_w = 1200$ K (assumed), constant-area section length of 2.6 m, combustor expansion length of 3.17 m, and a combustor expansion angle of 8.9 deg. The preceding conditions and geometry are provided as an example and do not imply any optimality.

The resulting distributions in Mach number and pressure are shown in Fig. 9. The Mach number is observed to decrease sharply as a result of mass injection at the beginning of the combustor. At a distance of approximately 0.25 m, fuel ignition is observed with another sharp decrease in Mach number. The Mach number further decreases beyond fuel ignition as a result of combustion and friction effects. At the end of the strut, the sharp rise in Mach number is caused by the expansion from the base of the strut. The Mach number then further rises after the strut as a result of the constant angle expansion region of the combustor. The pressure trend mirrors the effects of the Mach number trend (as Mach number goes down, pressure increases).

The resulting distributions in temperature and mass fractions of H_2O, OH, and NO are shown in Fig. 10. A rise in temperature is observed for both mass injection and for fuel ignition in the same manner as Mach number. After the strut injector base the temperature rises instead of falls, as would be expected in a supersonic expansion. Observing the water mass fraction, it is seen that at the strut base expansion water is being created. Because of the high combustion temperatures in the constant-area region of the combustor, dissociation of water is occurring (observe the OH mass fraction). When the flow cools down through the initial expansion, water can begin to form. As the expansion becomes less severe (i.e., after the base), the heat release from water formation is still high enough to

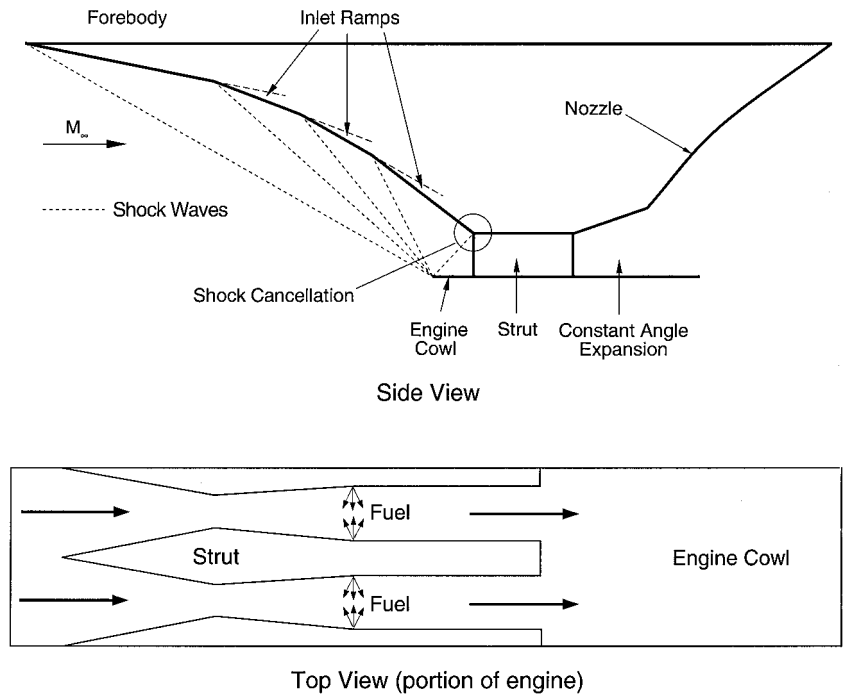

Fig. 8 RBCC engine geometry, top and side view (not to scale).

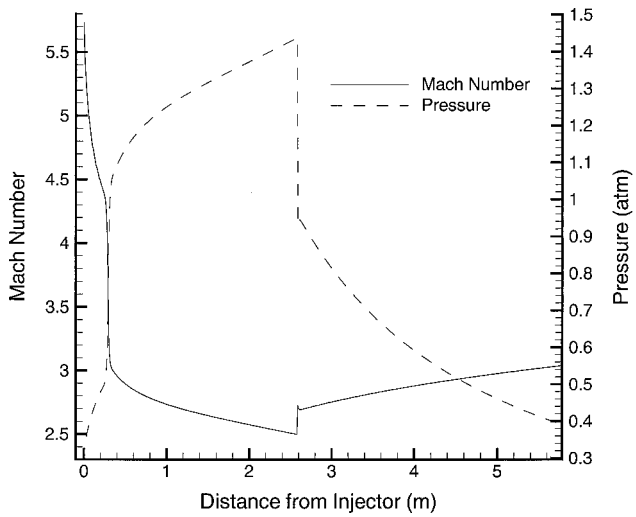

Fig. 9 Mach number and pressure distribution in rocket-based combined-cycle engine.

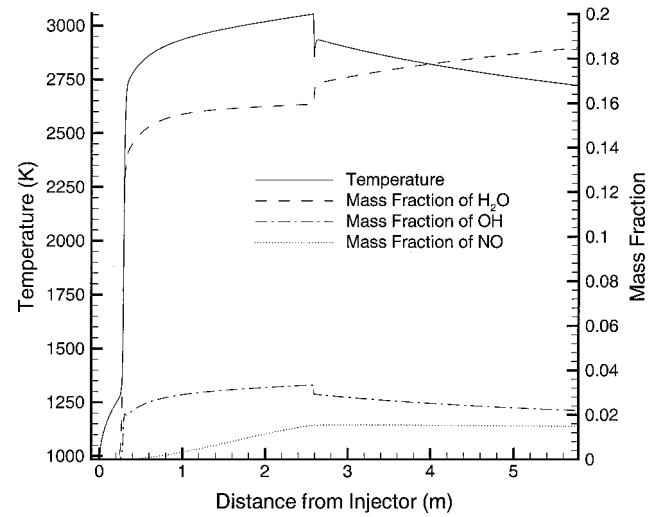

Fig. 10 Temperature and mass fraction of H_2O, OH, and NO distribution in rocket-based combined-cycle engine.

heat the flow. As the flow continues in the expansion region, less reactions occur, and the mass fraction begins to level out. Consequently, the temperature begins to fall as a result of the expansion, with the expected result of temperature decrease in a supersonic expansion.

The combustion efficiency in this study is defined as the mole fraction of water at the exit of the combustor divided by the stoichiometric mole fraction of water if all of the hydrogen had been converted to water. In this manner the combustion efficiency for this particular case was found to be about 69%. This low value of combustion efficiency is partially caused by the high combustion temperatures (~3000 K) in the burner keeping some of the water dissociated and to the formation of NO (see Fig. 10) that reduces the amount of available oxygen for reaction. The low value of efficiency is also a result of the high expansion angle used in the combustor, freezing the reactions before completion.

The primary indicator of engine performance used in this study is specific impulse, defined in the simplest form as $I_{sp} = T/(\dot{m}_f g)$. If the net thrust is used (for accelerator vehicles), the effective specific impulse is defined as $I_{sp,eff} = (T - D)/(\dot{m}_f g)$. The effective overall propulsion specific impulse (the effective specific impulse including all components that come in contact with the flowfield entering and leaving the combustor) was found to be 821 s. The effective propulsion specific impulse (the effective overall propulsion specific impulse not including the compression components prior to the engine cowl) was found to be 1312 s. Finally, the propulsion specific impulse (total thrust generated by the engine and nozzle) was found to be 2509 s. These values are all partially dependent on the calculation of strut base pressure, which will affect the thrust generated on each strut.

Application: Hydrocarbon Missile Scramjet Engine

The finite-rate chemistry engine model developed in this paper is applied to a Mach 8 missile with a hydrocarbon-burning scramjet engine, as shown in Fig. 11. The modeling methodologies used in developing this missile application are not shown in this paper.[21,22]

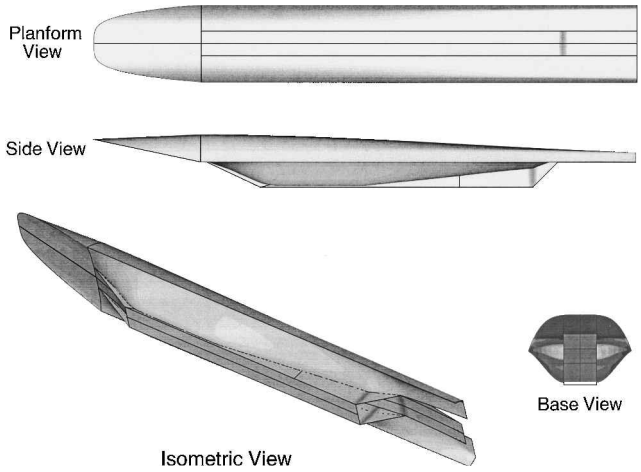

Fig. 11 Example hydrocarbon scramjet missile geometry.

The scramjet used for this application was two dimensional with constant area for the first half of the combustor and had a constant expansion angle for the second half of the combustor. The inlet to this engine was a series of three, two-dimensional ramps following the forebody compression. Similar to the rocked-based combined-cycle model described in the preceding section, the compression shocks all converge at the cowl lip where the flow is then turned parallel to freestream with the resulting cowl shock being cancelled at an expansion corner at the entrance to the combustor. This results in a uniform flowfield at the combustor entrance for inviscid flow. Upon exit from the combustor, the flow is expanded using a two-dimensional nozzle, which is analyzed using the method of characteristics.[20]

The internal components in the combustor follow those outlined in Fig. 2 with the fuel injection taking place between $x_{\text{inj},s}$ and $x_{\text{inj},e}$ and a prescribed mixing length L_{mix}, where the fuel becomes sufficiently mixed with the incoming air for combustion to take place. Also, a mixing efficiency η_{mix} is used to describe the effects caused by ineffective mixing and allows unburned fuel to pass through the combustor.

The Jet-A fuel reaction mechanism is modeled using a reduced reaction mechanism developed by Kundu et al.,[9] where the Jet-A fuel is modeled as $C_{12}H_{23}$ with a density of $\rho_f = 855$ kg/m^3. The reduced mechanism consists of 17 species and 14 reactions and was chosen because it has been validated for scramjet applications by Chang[10] and Lewis and Chang[11] and shown to have good agreement with the full mechanism for both ignition times and pressure rise for a number of different equivalence ratios.

In the example missile shown in Fig. 11, the inlet conditions into the combustor are $p = 1.519$ atm, $T = 1335$ K, $M = 2.563$, $\gamma = 1.318$, $\dot{m} = 2.435$ kg/s, $\dot{m}_f = 0.152$ kg/s, $\phi = 0.929$, $T_w = 1200$ K (assumed), $\eta_{\text{mix}} = 90\%$ (assumed), $x_{\text{inj},s} = 0.2$ m, $x_{\text{inj},e} = 0.3$ m, $L_{\text{mix}} = 0.5$ m, constant-area section length of 0.745 m, combustor expansion length of 0.745 m, and a combustor expansion angle of 8.39 deg.

The Mach number and pressure distribution for the missile scramjet engine are shown in Fig. 12. The figure shows the Mach number slowly decreasing (caused by viscous effects) until the fuel injection starts at $x = 0.2$ m. There is a sharp drop in Mach number where the injection starts, then the curve resumes a steady downward trend. At about 0.7 m the fuel ignition begins (this is the distance of $x_{\text{inj},s} + L_{\text{mix}}$), and there is another sharp drop in Mach number until the throat is reached at $x = 0.745$ m. Expansion is shown to initially increase the Mach number after the throat, but then the effects of heat release are shown to overtake the expansion effects and the Mach number drops for a short distance. In the remainder of the expansion portion of the combustor, the Mach number increases. The pressure distribution is almost a mirror image of the Mach-number distribution.

The temperature profile and mass fractions of H_2O, CO_2, and NO for the missile are shown in Fig. 13. The temperature is shown

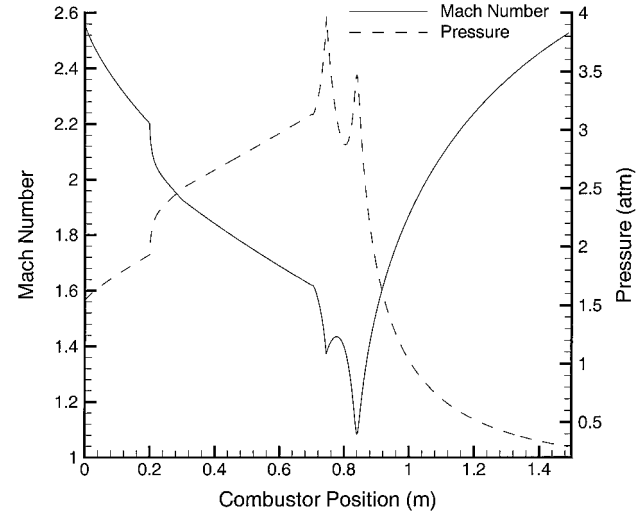

Fig. 12 Mach number and pressure distribution in missile scramjet engine.

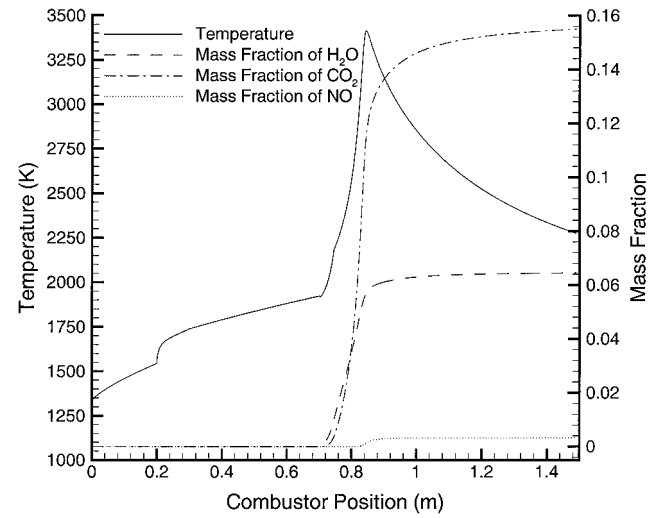

Fig. 13 Temperature and H_2O, CO_2, and NO mass fraction distribution in missile scramjet engine.

to increase steadily until the point of ignition with a slight jump caused by the fuel injection. Once ignition occurs, the temperature rises about 1500 K (even through the expansion effects of the throat) after which it drops steadily as the flow is expanded supersonically in the second half of the combustor. As the combustion progresses, the production of the H_2O, CO_2, and NO species occurs as expected. The CO_2 mass fraction continues a slow rise in the expansion portion of the combustor, indicating that the flow does not freeze through the throat and that combustion is incomplete at the end of the combustor.

A combustion efficiency is used for the hydrocarbon scramjet engine, which is based on the amount of water and carbon dioxide exiting the combustor relative to the amount of water and carbon dioxide which would exit a stoichiometric combustor (if all of the fuel and oxygen had been transformed to H_2O and CO_2):

$$\eta_{\text{comb}} = \frac{X_{H_2O} + X_{CO_2}}{[X_{H_2O} + X_{CO_2}]_{\text{st}}} \tag{39}$$

Using this approach, the combustion efficiency for this example combustor was found to be 74.5%. This low efficiency is caused by a slightly lean equivalence ratio, a mixing efficiency of only 90%, ignition just prior to flow expansion, and short combustor length.

The specific impulse achieved by this engine-integrated missile design was 1894 s. The effective overall propulsion specific impulse was 334 s, and the propulsion specific impulse was 2478 s.

Summary

A quasi-one-dimensional high-speed engine model with finite-rate chemistry has been presented. Rapid and accurate prediction of fuel ignition and pressure profiles have been demonstrated, compared to previous experiments. The full aerodynamic and chemical flowfield of a rocket-based combined-cycle engine and a hydrocarbon-fueled missile scramjet were shown as specific applications of the engine model. These applications were selected to demonstrate the applicability of the model to cases where equilibrium assumptions are invalid.

Because of the one-dimensional nature of the engine model, rapid engine prediction allows for full vehicle optimization that can include a detailed combustor. The primary weakness of this model is the assumed mixing profile, which is inherently a function of the flowfield, injector geometry, fuel, and many other factors. However, considering the substantial limitations of quasi-one-dimensional flow, the model does an excellent job of predicting the complex phenomena involved in high-speed combustion.

Acknowledgments

This research was supported by NASA John H. Glenn Research Center under Grant NAG32480, with technical monitor Don Palac, to whom appreciation is expressed.

References

[1]Shapiro, A., *The Dynamics and Thermodynamics of Compressible Fluid Flow*, Vol. 1, Ronald, New York, 1953, pp. 219–260.

[2]Eckert, E. R. G., "Engineering Relations for Friction and Heat Transfer to Surfaces in High Velocity Flow," *Journal of the Aeronautical Sciences*, Vol. 22, 1955, pp. 585–587.

[3]White, F. M., *Viscous Fluid Flow*, 1st ed., McGraw–Hill, New York, 1974, pp. 28, 29, 511.

[4]Turns, S. R., *An Introduction to Combustion*, 1st ed., McGraw–Hill, New York, 1996, pp. 151–207.

[5]Kee, R. J., Rupley, F. M., and Miller, J. A., "CHEMKIN-II: A Fortran Chemical Kinetics Package for the Analysis of Gas Phase Chemical Kinetics," SAND 89-8009B, Sandia National Labs., Albuquerque, NM, April 1989.

[6]Eckert, E. R. G., "Engineering Relations for Heat Transfer and Friction in High-Velocity Laminar and Turbulent Boundary-Layer Flow over Surfaces with Constant Pressure and Temperature," *Transactions of the ASME*, Vol. 78, No. 6, 1956, p. 1273.

[7]Byrne, G. D., Hindmarch, A. C., and Brown, P. N., "VODPK: Variable-Coefficient Ordinary Differential Equation Solver with the Preconditioned Krylov Method GMRES for the Solution of Linear Systems," Lawrence Livermore National Lab., Livermore, CA, May 1997.

[8]Jachimowski, C. J., "An Analytical Study of the Hydrogen-Air Reaction with Application to Scramjet Combustion" NASA TP 2791, Feb. 1988.

[9]Kundu, K. P., Penko, P. F., and Yang, S. L., "Reduced Reaction Mechanism for Numerical Calculations in Combustion of Hydrocarbon Fuels," AIAA Paper 98-0803, Jan. 1998.

[10]Chang, J. S., "Development of a Jet-A/Silane/Hydrogen Reaction Mechanism for Modeling a Scramjet Combustor," Dept. of Aerospace Engineering, Univ. of Maryland, College Park, May 1999.

[11]Lewis, M. J., and Chang, J. S., "Joint Jet-A/Silane/Hydrogen Reaction Mechanism," *Journal of Propulsion and Power*, Vol. 16, No. 2, 2000, pp. 365–367.

[12]Billig, F. S., and Grenleski, S. E., "Heat Transfer in Supersonic Combustion Processes," *Heat Transfer 1970*, edited by U. Grigull and E. Hahne, Vol. 3, Elsevier, Amsterdam, 1970, pp. 1–11.

[13]Heiser, W., and Pratt, D., *Hypersonic Airbreathing Propulsion*, AIAA, Washington, DC, 1994, pp. 251–256, 362–370.

[14]Pinckney, S. Z., "Turbulent Heat Transfer Prediction Method for Application to Scramjet Engines," NASA TN D-7810, Nov. 1974.

[15]Rogers, R. C, "Mixing of Hydrogen Injected from Multiple Injectors Normal to a Supersonic Airstream," NASA TN D-6476, Sept. 1971.

[16]Henry, J. R., and Anderson, G. Y., "Design Considerations for the Airframe-Integrated Scramjet," NASA TM X-2895, Dec. 1973.

[17]Anderson, G. Y., and Gooderum, P. B., "Exploratory Tests of Two Strut Fuel Injectors for Supersonic Combustion," NASA TN D-7581, Feb. 1974.

[18]Siebenhaar, A., and Bulman, M., "The Strutjet Engine: The Overlooked Option for Space Launch," AIAA Paper 95-3124, July 1995.

[19]O'Brien, T. F., and Lewis, M. J., "RBCC Engine-Airframe Integration on an Osculating Cone Waverider Vehicle," AIAA Paper 2000-3823, July 2000.

[20]Anderson, J. D., *Modern Compressible Flow: With Historical Perspective*, McGraw–Hill, New York, 1990, pp. 311–331.

[21]Starkey, R. P., "Investigation of Air-Breathing, Hypersoic Missile Configurations Within External Box Constraints," Ph.D. Dissertation, Dept. of Aerospace Engineering, Univ. of Maryland, College Park, Oct. 2000.

[22]Starkey, R. P., and Lewis, M. J., "Sensitivity of Hydrocarbon Combustion Modeling for Hypersonic Missile Design," AIAA Paper 2000-3312, July 2000.